Supporting Information

Selectivity Control in Palladium-Catalyzed CH_2Br_2 Hydrodebromination on Carbon-Based Materials by Nuclearity and Support Engineering

Matteo Vanni,[§,‡] *Vera Giulimondi,*[§,‡] *Andrea Ruiz-Ferrando,*[†,#] *Frank Krumeich,*[§] *Adam H. Clark,*[¥] *Sharon Mitchell,*[§] *Núria López,*[†] *Javier Pérez-Ramírez*[§,*]

[§] Institute for Chemical and Bioengineering, Department of Chemistry and Applied Biosciences, ETH Zurich, Vladimir-Prelog-Weg 1, 8093 Zurich, Switzerland.

[†] Institute of Chemical Research of Catalonia (ICIQ-CERCA), The Barcelona Institute of Science and Technology, Av. Països Catalans 16, 43007 Tarragona, Spain.

[#] Departament de Química Física i Inorgànica, Universitat Rovira i Virgili, Marcel·lí Domingo s/n, 43007 Tarragona, Spain.

[¥] Photon Science Division, Paul Scherrer Institute, 5232 Villigen, Switzerland.

[‡] Equal contribution.

* Corresponding author. E-mail: jpr@chem.ethz.ch.

Table S1. Fitting parameters derived from the Pd *K*-edge EXAFS spectra of selected catalysts in fresh form.

Catalyst	Coordination	CN[a] / -	σ^{2b} / Å^2	R^c / Å
Pd_{NP}/AC	Pd-C/N/O	0.7 ± 0.2	0.003 ± 0.002	1.80 ± 0.02
	Pd-C/N/O	1.5 ± 0.2	0.003 ± 0.002	1.96 ± 0.02
	Pd-Cl	0.8 ± 0.3	0.002[d]	2.28 ± 0.02
	Pd-Pd	6.8 ± 0.6	0.008 ± 0.001	2.78 ± 0.01
Pd_{SA}/AC	Pd-C/N/O	0.7 ± 0.2	0.003 ± 0.002	2.05 ± 0.02
	Pd-Cl	2.9 ± 0.3	0.002[d]	2.31 ± 0.02
Pd_{SA}/NC	Pd-C/N/O	1.3 ± 0.2	0.002 ± 0.002	1.88 ± 0.02
	Pd-C/N/O	3.1 ± 0.3	0.002 ± 0.002	2.02 ± 0.02
	Pd-Pd	0.4 ± 0.2	0.007 ± 0.003	2.78 ± 0.03
	Pd-C/N/O	0.8 ± 0.3	0.002 ± 0.002	2.84 ± 0.02
Pd_{SA}/ECN	Pd-C/N/O	4.3 ± 0.5	0.002 ± 0.002	2.02 ± 0.02
	Pd-Pd	0.8 ± 0.2	0.005 ± 0.002	2.70 ± 0.03
	Pd-C/N/O	3.2 ± 0.3	0.002 ± 0.002	2.96 ± 0.03
Pd_{SA}/PTI	Pd-C/N/O	4.7 ± 0.4	0.002 ± 0.002	2.01 ± 0.02
	Pd-Pd	0.6 ± 0.2	0.005 ± 0.002	2.72 ± 0.03
	Pd-C/N/O	4.6 ± 0.5	0.002 ± 0.002	2.96 ± 0.04

[a]Coordination number. [b]Debye-Waller factor. [c]Coordination shell distance. [d]Fixed parameter based on the refinement of the $PdCl_2$ reference.

Table S2. Fitting parameters derived from the Pd K-edge EXAFS spectra of selected catalysts in used form.

Catalyst	Coordination	CN[a] / -	σ^{2b} / Å^2	R^c / Å
Pd_{NP}/AC-u	Pd-C/N/O	0.7 ± 0.2	0.003 ± 0.002	1.98 ± 0.02
	Pd-Br	1.2 ± 0.2	0.002[d]	2.42 ± 0.02
	Pd-Pd	6.5 ± 0.6	0.008 ± 0.001	2.79 ± 0.01
Pd_{SA}/AC-u	Pd-C/N/O	0.7 ± 0.2	0.003 ± 0.002	2.00 ± 0.03
	Pd-Br	1.8 ± 0.3	0.002[d]	2.42 ± 0.02
	Pd-Pd	5.3 ± 0.6	0.008 ± 0.001	2.78 ± 0.01
Pd_{SA}/NC-u	Pd-C/N/O	0.9 ± 0.2	0.003 ± 0.002	1.86 ± 0.03
	Pd-C/N/O	2.3 ± 0.3	0.003 ± 0.002	2.02 ± 0.02
	Pd-Br	1.3 ± 0.2	0.002[d]	2.44 ± 0.01
	Pd-Pd	0.4 ± 0.2	0.007 ± 0.003	2.82 ± 0.02
	Pd-C/N/O	0.8 ± 0.2	0.003 ± 0.002	2.91 ± 0.03
Pd_{SA}/ECN-u	Pd-C/N/O	2.3 ± 0.2	0.002 ± 0.002	2.01 ± 0.02
	Pd-Br	0.9 ± 0.2	0.002[d]	2.44 ± 0.03
	Pd-Pd	1.0 ± 0.2	0.005 ± 0.002	2.84 ± 0.02
	Pd-C/N/O	1.3 ± 0.2	0.002 ± 0.002	2.95 ± 0.04
Pd_{SA}/PTI-u	Pd-C/N/O	3.2 ± 0.3	0.003 ± 0.002	2.03 ± 0.01
	Pd-Br	0.9 ± 0.2	0.002[d]	2.45 ± 0.02
	Pd-Pd	1.1 ± 0.2	0.005 ± 0.002	2.79 ± 0.03
	Pd-C/N/O	4.3 ± 0.4	0.003 ± 0.002	3.01 ± 0.04

[a]Coordination number. [b]Debye-Waller factor. [c]Coordination shell distance. [d]Fixed parameter based on the refinement of the $PdBr_2$ reference.

Table S3. Fitting parameters derived from the Pd 3*d* XPS spectra of selected catalysts.

Catalyst	Pd(IV)[a]			Pd(II)[a]			Pd(0)[a]			C 1*s* reference / eV
	Position / eV	FWHM[b] / eV	Area / %	Position / eV	FWHM[b] / eV	Area / %	Position / eV	FWHM[b] / eV	Area / %	
Pd_{SA}/AC	338.6	2.5	21.3	337.0	2.2	78.7	-	-	-	284.8
Pd_{SA}/AC-u	338.6	2.5	22.4	336.8	1.8	41.0	335.7	1.7	36.6	284.8
Pd_{SA}/NC	338.3	1.7	44.0	337.2	1.4	56.0	-	-	-	284.8
Pd_{SA}/NC-u	338.3	2.4	38.7	337.2	1.5	61.3	-	-	-	284.8
Pd_{SA}/ECN	338.6	1.9	80.6	336.8	1.6	19.4	-	-	-	288.3
Pd_{SA}/ECN-u	338.6	2.0	40.6	337.2	1.7	24.5	335.7	2.5	34.9	288.3
Pd_{SA}/PTI	338.4	1.9	100.0	-	-	-	-	-	-	288.3
Pd_{SA}/PTI-u	338.4	2.5	70.9	337.2	2.4	29.1	-	-	-	288.3

[a]Assigned based on reported values.[1,2] [b]FWHM: full width at half maximum.

Table S4. Elemental surface concentrations of selected catalysts as determined by XPS.

Catalyst	C / at.%	N / at.%	O / at.%	Cl / at.%	Br / at.%
Pd_{SA}/AC	96.0	-	3.6	0.4	-
Pd_{SA}/AC-u	96.7	-	3.0	-	0.3
Pd_{SA}/NC	89.2	7.2	3.6	-	-
Pd_{SA}/NC-u	91.7	6.0	1.9	-	0.4
Pd_{SA}/ECN	43.5	55.5	1.0	-	-
Pd_{SA}/ECN-u	53.5	44.2	1.8	-	0.5
Pd_{SA}/PTI	45.4	50.5	4.0	0.1	-
Pd_{SA}/PTI-u	58.5	35.1	3.0	0.3	3.1

Table S5. Simulated adsorption energy, $E_{ads}(PdCl_x)$ in eV, of $PdCl_x$ (x = 0-4) species over distinct N-cavities in the NC support.

Metal species[a]	NC cavity	
	3×N5	4×N6
Pd	−4.22	−5.99
PdCl	−4.27	−4.53
$PdCl_2$	−4.03	−3.08
$PdCl_3$	−4.12	−2.17
$PdCl_4$	−1.43	−1.58

[a] $E_{ads}(PdCl_x)$ is calculated according to $E_{ads}(PdCl_x) = E_{ads}(PdCl_x, NC) - E(PdCl_x, g) - E(NC)$, where $E_{ads}(PdCl_x, NC)$ is the energy of the N-cavity with adsorbed $PdCl_x$, $E(PdCl_x)$ is the energy of the isolated $PdCl_x$ fragment and $E(NC)$ is the energy of the free N-cavity considered.

Table S6. Boltzmann population, in %, of $PdCl_x$ (x = 0-4) species over distinct N-cavities in the NC support.

Metal species[a]	NC cavity	
	3×N5	4×N6
Pd	7.6	92.4
PdCl	41.0	59.0
$PdCl_2$	79.4	20.6
$PdCl_3$	94.0	6.0
$PdCl_4$	44.7	55.3

[a]The population shown in the Table, calculated for chlorinated species, can be equated to that of the corresponding non-chlorinated Pd atom obtained upon thermal annealing, under the assumption that no redistribution of the $PdCl_x$ fragments takes place following their coordination to the host.

Table S7. Simulated dissociative adsorption energy of H_2, E_{diss}(H-H) on Pd single atoms stabilized on PTI, ECN, and NC.

Catalyst[a]	E_{diss}(H-H)[b] / eV
Pd_{SA}/PTI	−1.41
Pd_{SA}/ECN	−0.06
Pd_{SA}/NC (3×N5)	−1.32
Pd_{SA}/NC (4×N6)	0.65

[a]The optimized structure of each active site is shown in **Figure S15**. [b] E_{diss}(H-H) is calculated according to $E_{diss} = E_{ads} - E_{Pd\ site} - E_{gas}$, where E_{ads} is the energy of the active site with adsorbed H*/H$^{\#}$, $E_{Pd\ site}$ is the energy of the free Pd active site, and E_{gas} is the energy of gas-phase H_2, respectively.

Table S8. Simulated Gibbs free energy, G of the intermediates shown in **Figure 8**.

Catalyst[a]	Intermediate	*G* / eV
Pd_{SA}/PTI	CH_2Br_2 (g) + H*+ $H^{\#}$	0.00
	$CH_2Br_2^{\#}$+ H* + $H^{\#}$	0.01
	TS	1.24
	CH_3Br (g) + HBr (g)	−2.53
	CH_2* + HBr*	−0.34
	CH_2* + HBr (g)	−0.43
	$H^{\#}$ + H*	−1.59
Pd_{SA}/ECN	CH_2Br_2 (g) + H_2 (g)	0.00
	CH_2Br_2 + H* + $H^{\#}$	0.88
	$CH_2Br_2^{\#}$ + H* + $H^{\#}$	0.29
	TS	0.55
	CH_3Br (g) + HBr (g)	−0.94
	CH_2*+ HBr*	0.13
	CH_2*+ HBr (g)	0.55
Pd_{SA}/NC	CH_2Br_2 (g) + H_2 (g)	0.00
	CH_2Br_2 + H* + $H^{\#}$	−0.43
	$CH_2Br_2^{\#}$ + H* + $H^{\#}$	−0.79
	TS	0.52
	CH_3Br (g) + HBr (g)	−0.94
	CH_2*+ HBr*	−0.38
	CH_2*+ HBr (g)	−0.03

[a]The optimized structure of each active site is shown in **Figure S15**.

Table S9. Simulated dissociative adsorption energy of H_2, E_{diss}(H-H), and corresponding kinetic barrier, R_{diss}(H-H), on monobrominated Pd single atoms stabilized on PTI, ECN, and NC.

Catalyst	E_{diss}(H-H)[a] / eV	R_{diss}(H-H)[b] / eV
Pd-Br/PTI	−1.41	0.71
Pd-Br/ECN	0.03	0.75
Pd-Br/NC (3×N5)	−0.07	1.71

[a] E_{diss}(H-H) is calculated according to $E_{diss}(H\text{-}H) = E_{ads} - E_{Pd\text{-}Br\ site} - E_{gas}$, where E_{ads} is the energy of the active site with adsorbed H-H, $E_{Pd\text{-}Br\ site}$ is the energy of the free Pd-Br active site, and E_{gas} is the energy of gas-phase CH_2Br_2 and H_2, respectively. [a] R_{diss}(H-H) is calculated according to $R_{diss}(H\text{-}H) = E_{TS}(H\text{-}H) - E_{Pd\text{-}Br\ site} - E_{gas}$, where E_{TS}(H-H) is the energy of the corresponding transition state.

Table S10. Span energy of the CH_2Br_2 HDB calculated for distinct Pd single atoms stabilized on PTI, ECN, and NC.

Catalyst	E_{span}[a] / eV
Pd_{SA}/PTI	1.24
Pd_{SA}/ECN	0.55
Pd_{SA}/NC (3×N5)	0.52

[a] E_{span} is calculated based on the steps shown in **Table S8.**

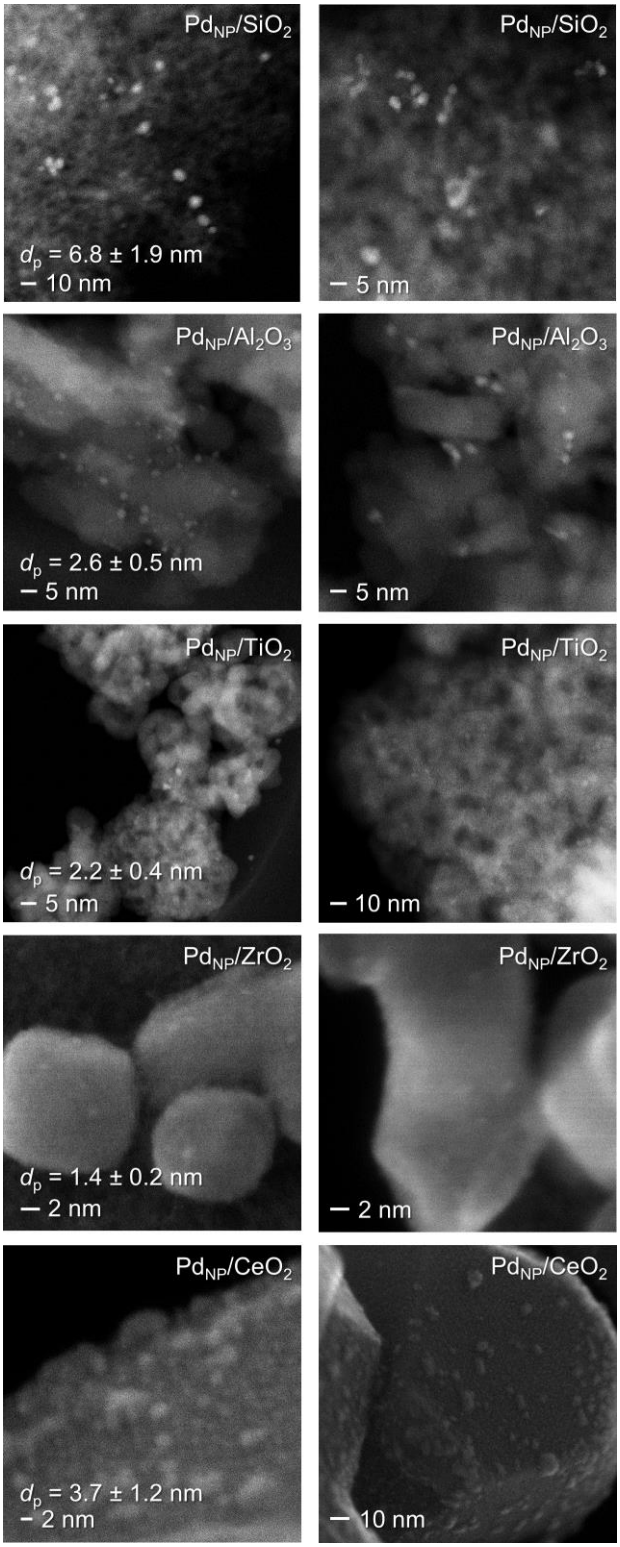

Figure S1. HAADF-STEM and SE-STEM micrographs of Pd NP supported on different metal oxides and corresponding mean particle size, d_p. SE-STEM was used for imaging Pd NP on oxidic supports (ZrO_2 and CeO_2) with low *Z*-contrast in HAADF-STEM.

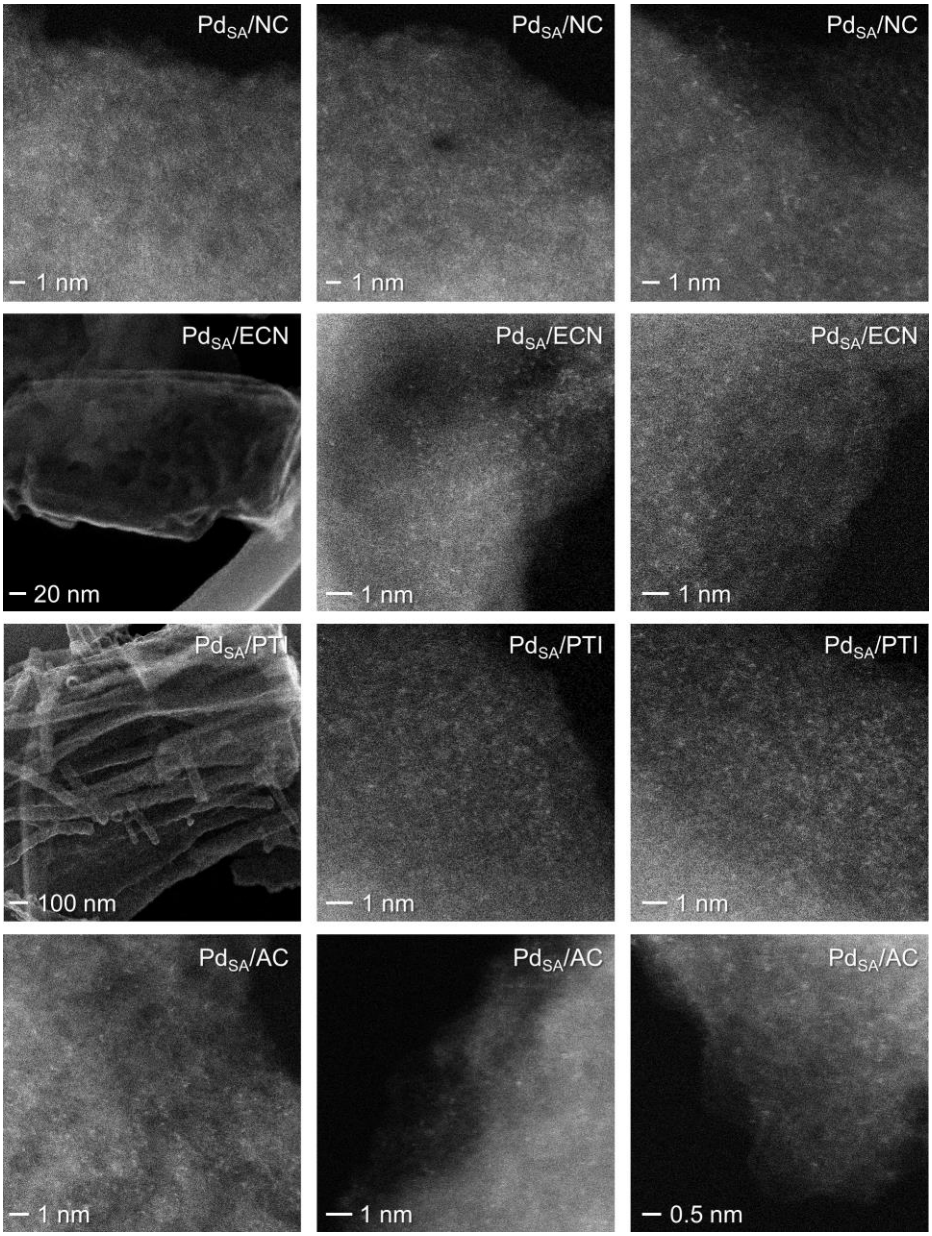

Figure S2. HAADF-STEM and SE-STEM micrographs of Pd SA supported on different carbon-based hosts, visualizing the metal atomic dispersion. SE-STEM was used for low-magnification imaging of the layered morphology of ECN and the crystalline nature of PTI (second and third row, respectively, left micrographs).

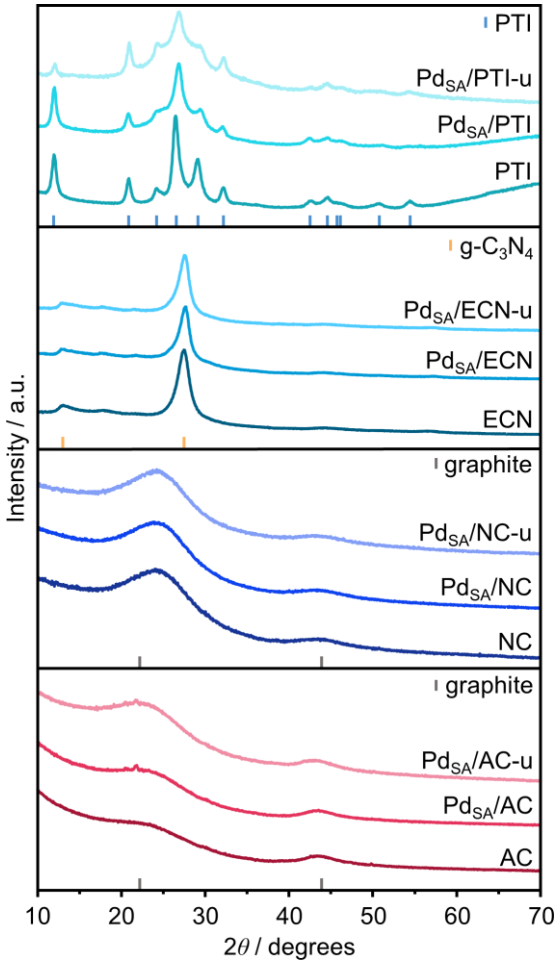

Figure S3. XRD patterns of Pd SA supported on different carbon-based hosts. No reflections related to the presence of a metallic Pd phase are detected in the spectra, in agreement with the atomic dispersion observed in HAADF-STEM (**Figure S2)**.

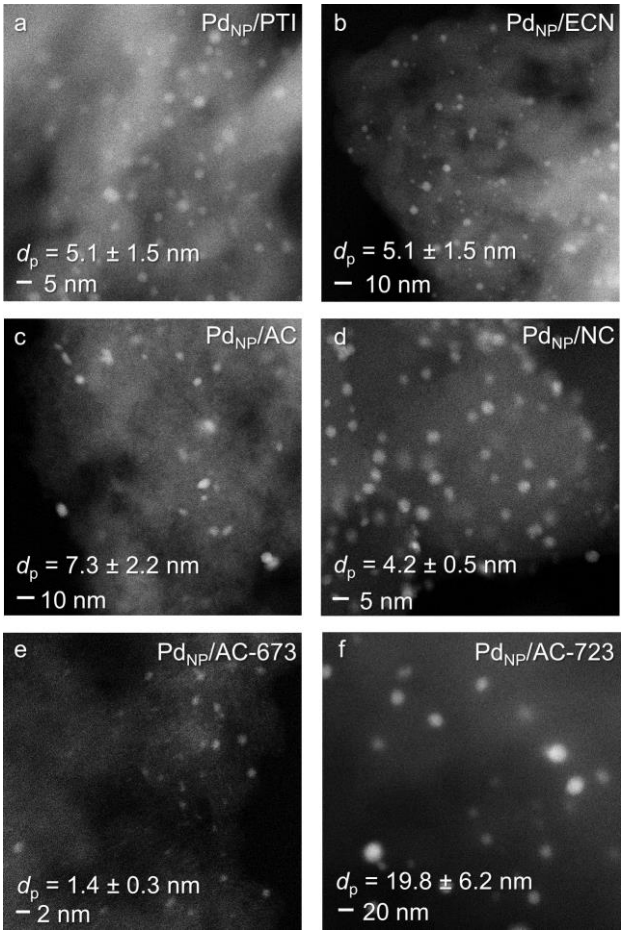

Figure S4. HAADF-STEM micrographs of Pd NP supported on different carbon-based hosts, synthesized via (**a-d**) reductive treatment and (**e-f**) harsh thermal activation in inert atmosphere of the impregnated catalysts.

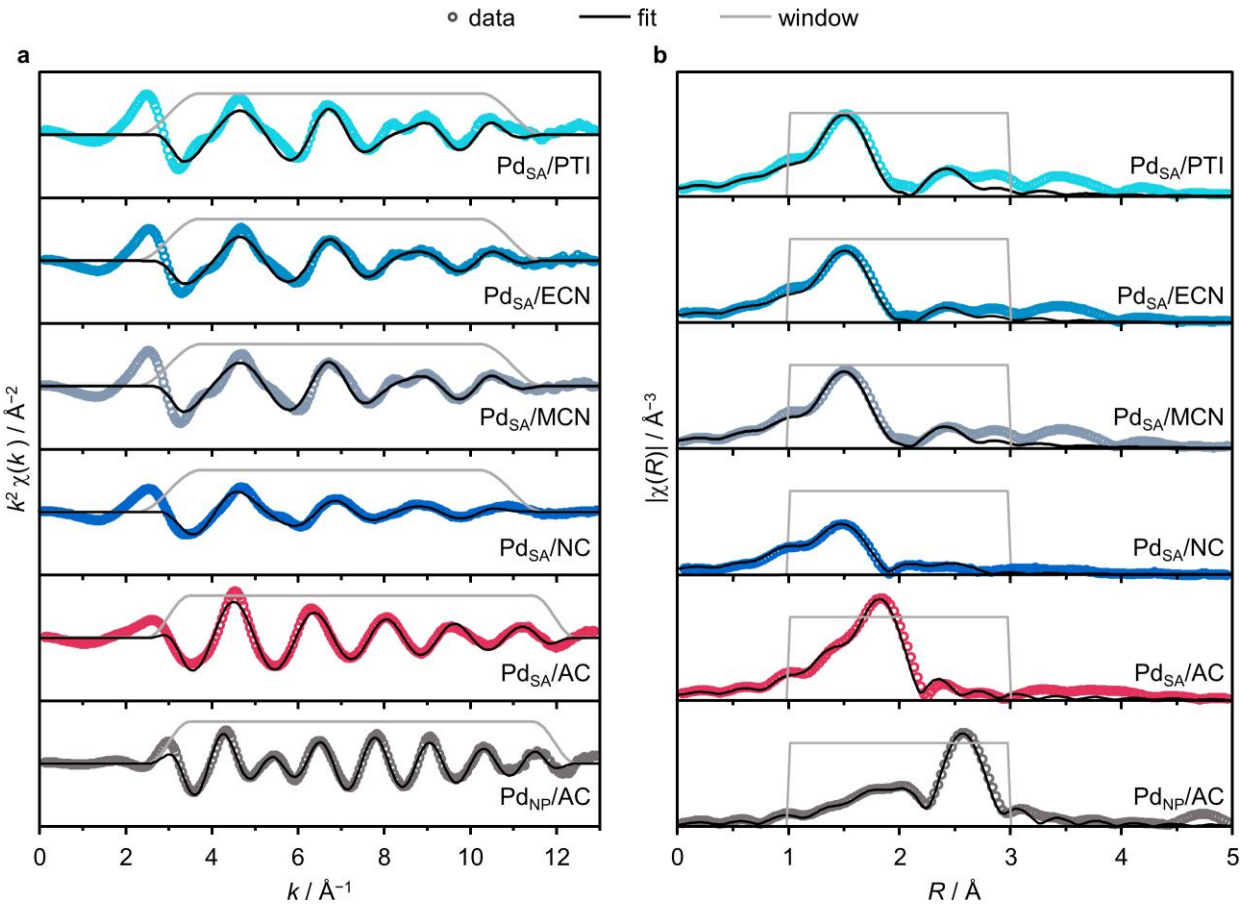

Figure S5. Experimental and fitted Pd *K*-edge EXAFS spectra of selected catalysts in fresh form. (**a**) *k*-space and (**b**) *R*-space.

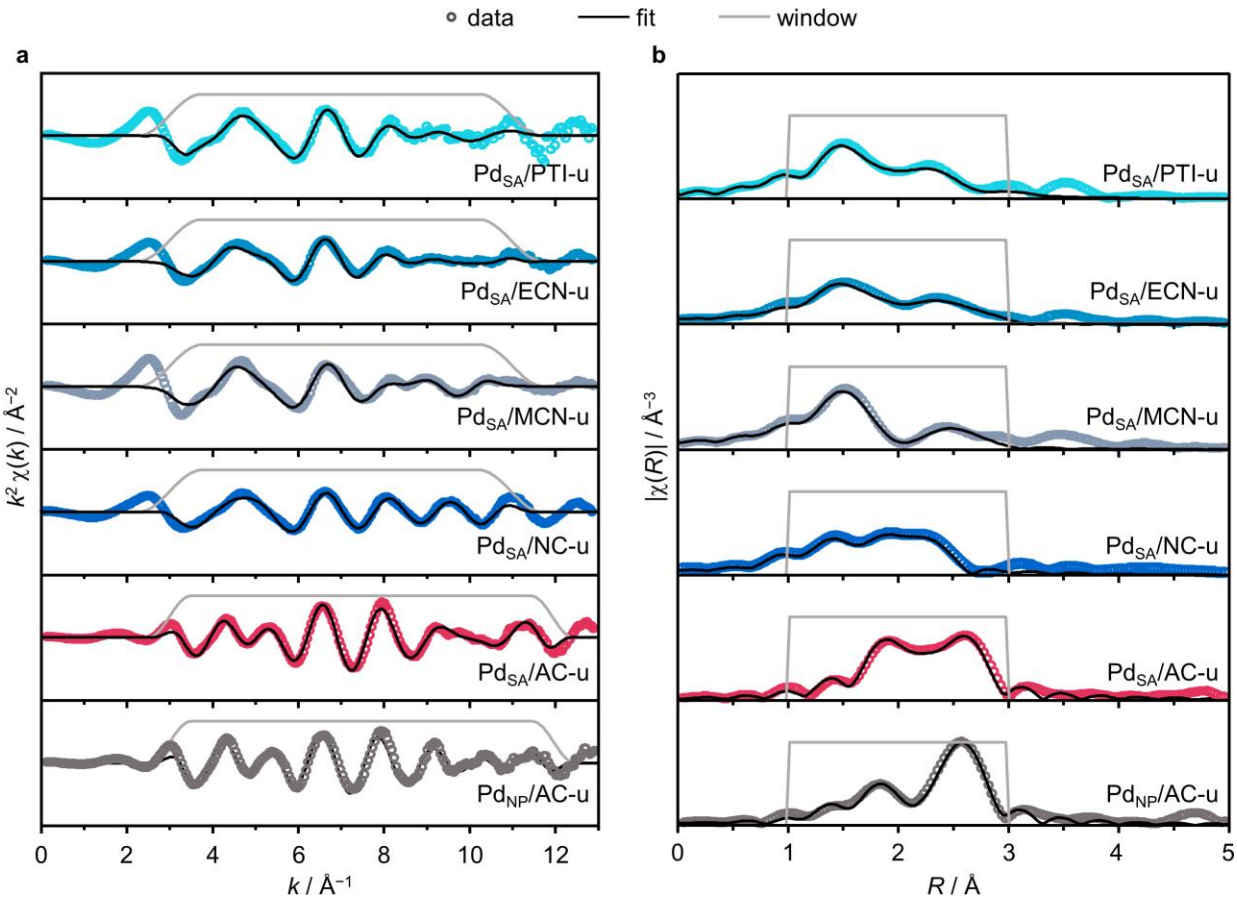

Figure S6. Experimental and fitted Pd *K*-edge EXAFS spectra of selected catalysts in used form. (**a**) *k*-space and (**b**) *R*-space.

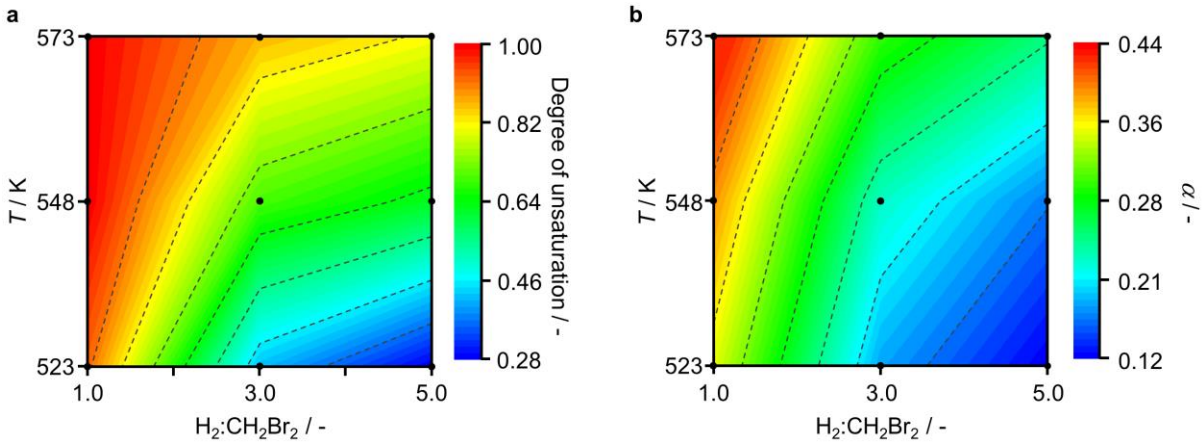

Figure S7. Product distribution over Pd_{NP}/SiO_2 as a function of varying CH_2Br_2 HDB conditions. (**a**) Degree of unsaturation of the formed hydrocarbons, mapping the yield in olefin products, and (**b**) chain growth probability, α mapped as a function of temperature and the H_2:CH_2Br_2 ratio. The chain growth probability is derived from Anderson-Schulz-Flory plots as described in the caption of **Figure S8**.[3]

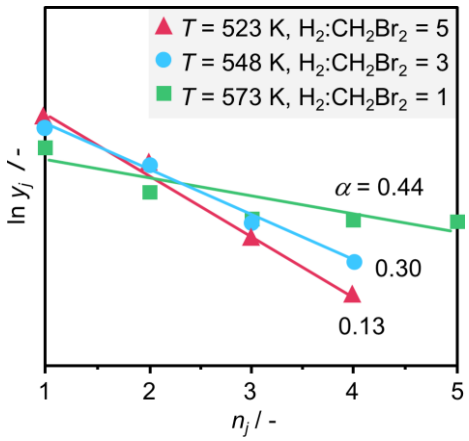

Figure S8. Representative Anderson-Schulz-Flory plots over Pd_{NP}/SiO_2 obtained by linear regression of concentration data, y_j as a function of the number of carbon atoms, n_j of each product j. The chain growth probability, α is determined as the natural exponential of the slope.[3]

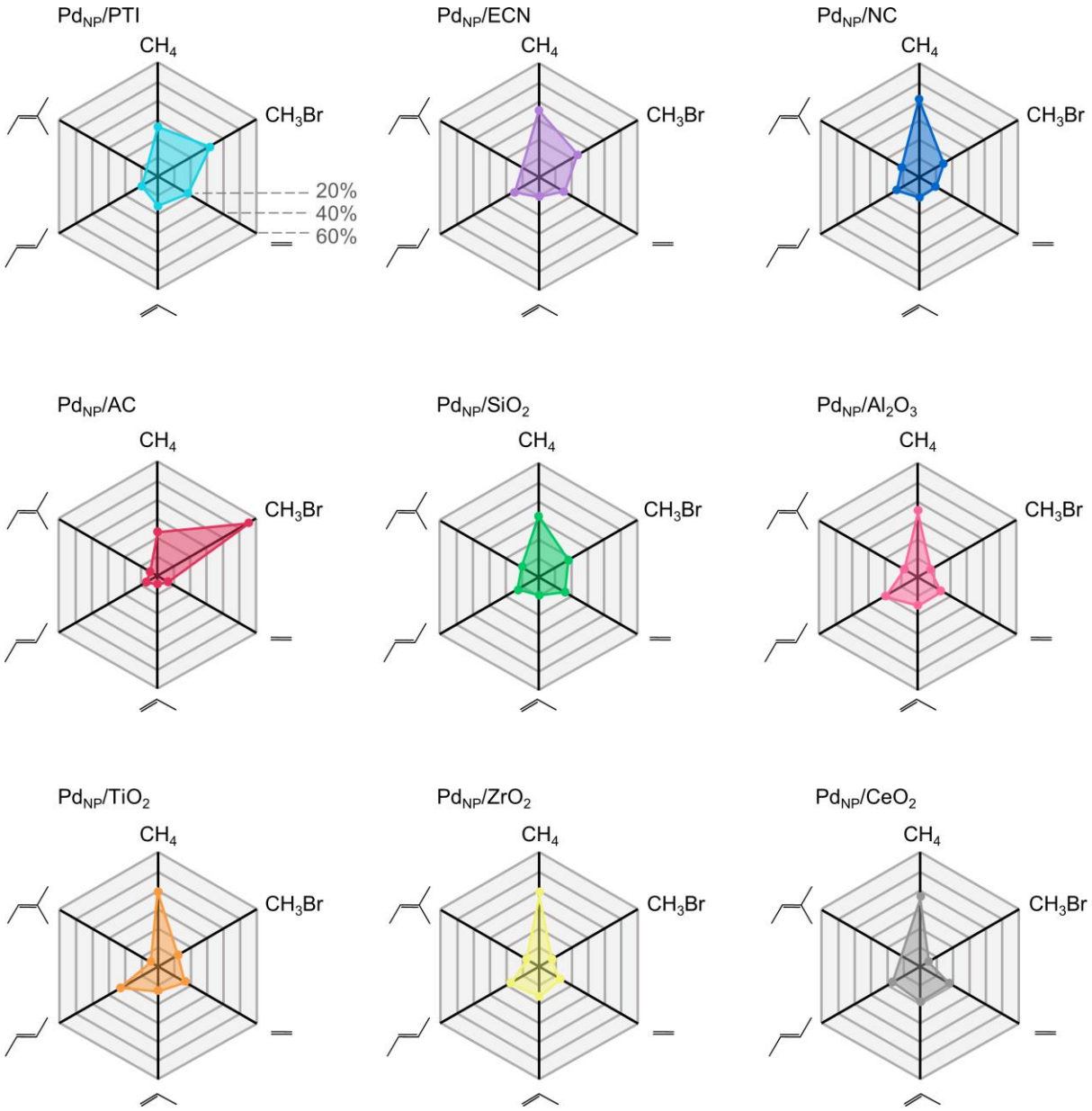

Figure S9. Product distribution over the Pd NP catalysts reported in **Figure 3**. The composition of the olefinic fraction is comparable for most of the catalysts studied. Reaction conditions: CH_2Br_2:H_2:Ar:He = 6:6:5:83, T = 573 K, P = 1 bar, $GHSV$ = 10800 $cm^3\ h^{-1}\ g_{cat}^{-1}$.

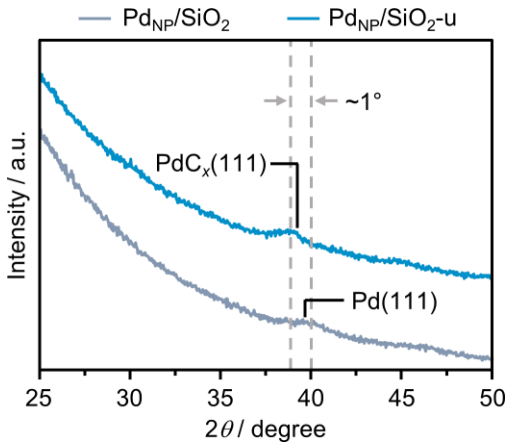

Figure S10. XRD patterns of fresh and used Pd_{NP}/SiO_2. Owing to the uptake of C upon exposure of metallic Pd NP to CH_2Br_2 with formation of a palladium carbide species, PdC_x a shift to lower angles in the position of the Pd(111) reflection is observed, resulting from lattice expansion.[3]

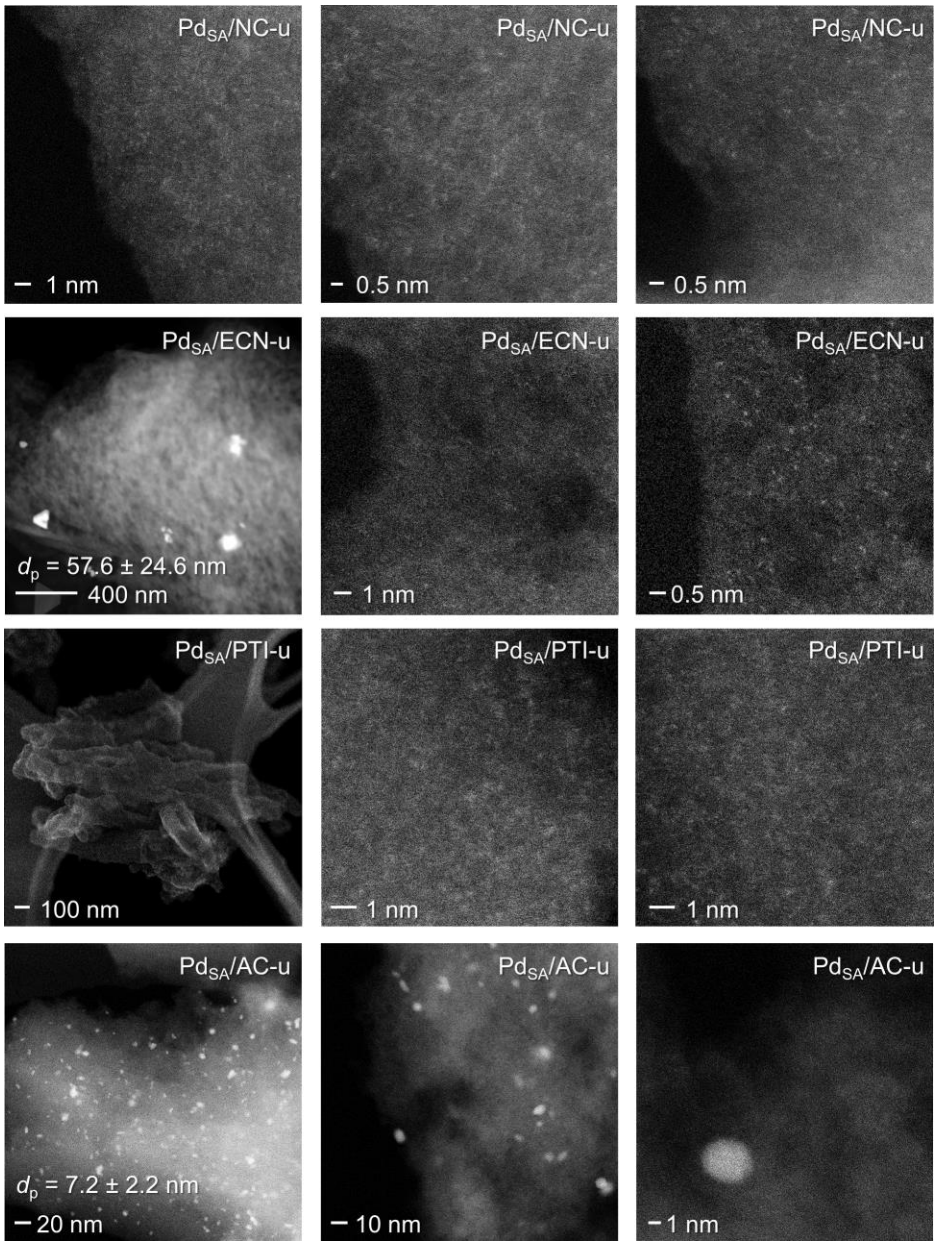

Figure S11. HAADF-STEM micrographs of the used Pd SA supported on different carbon-based hosts. Extensive sintering is observed for Pd$_{SA}$/AC-u. While Pd$_{SA}$/ECN-u features mainly atomically dispersed Pd, large metal aggregates are sporadically detected in the sample (second row, left).

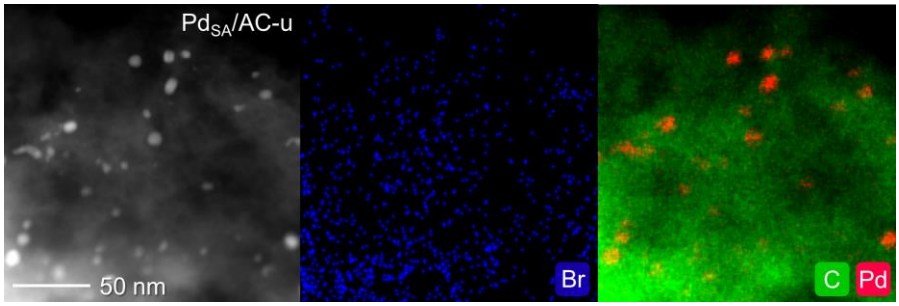

Figure S12. HAADF-STEM micrograph and corresponding elemental mapping by EDX (Br, C, and Pd) of the used Pd SA supported on AC. The weak intensity of the Br signal points to a limited uptake over time on stream.

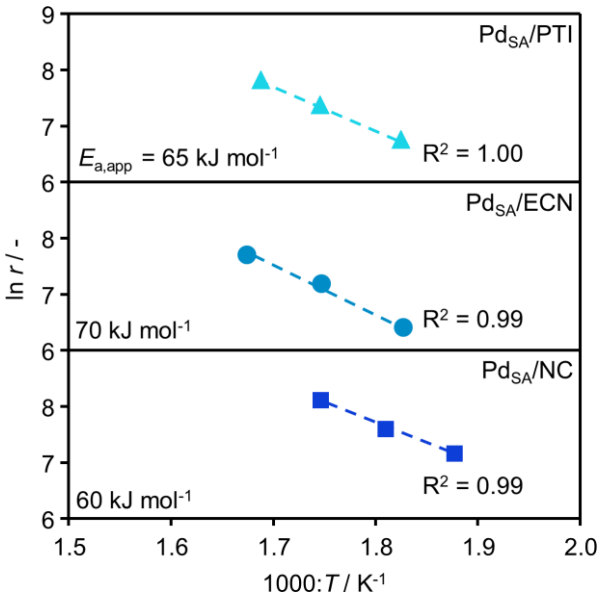

Figure S13. Arrhenius plot of CH_2Br_2 hydrodebromination over the Pd SA supported on different carbon-based hosts. Apparent activation energies are derived from linear regression of rate data within the temperature range T = 533-598 K. Other conditions: CH_2Br_2:H_2:Ar:He = 6:6:5:83, P = 1 bar, $GHSV$ = 1800-4320 cm^3 h^{-1} g_{cat}^{-1}.

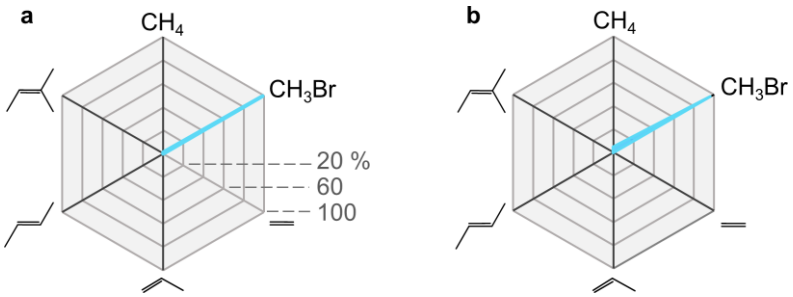

Figure S14. Evaluation of the effect of the carbon nitride host morphology on the product selectivity over supported Pd SA catalysts, comparing (**a**) mesoporous and (**b**) exfoliated carbon nitrides. No prominent differences are observed. Reaction conditions: CH_2Br_2:H_2:He:Ar = 6:6:83:5, T = 573 K, P = 1 bar, $GHSV$ = 900 $cm^3\ h^{-1}\ g_{cat}^{-1}$.

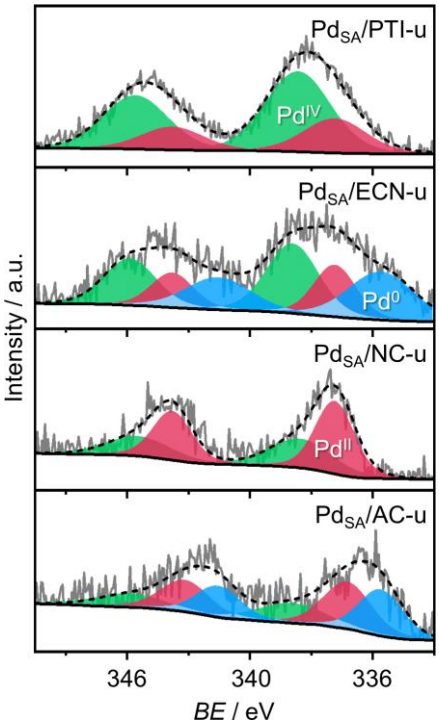

Figure S15. Pd 3*d* XPS spectra of the used Pd SA supported on carbon-based hosts. Pd SA stabilized on O-functionalities in AC suffer from sintering into NP, in line with HAADF-STEM and XAS analyses (**Figures S12** and **Table S4**). The formation of some reduced palladium is also observed for Pd SA supported on ECN.

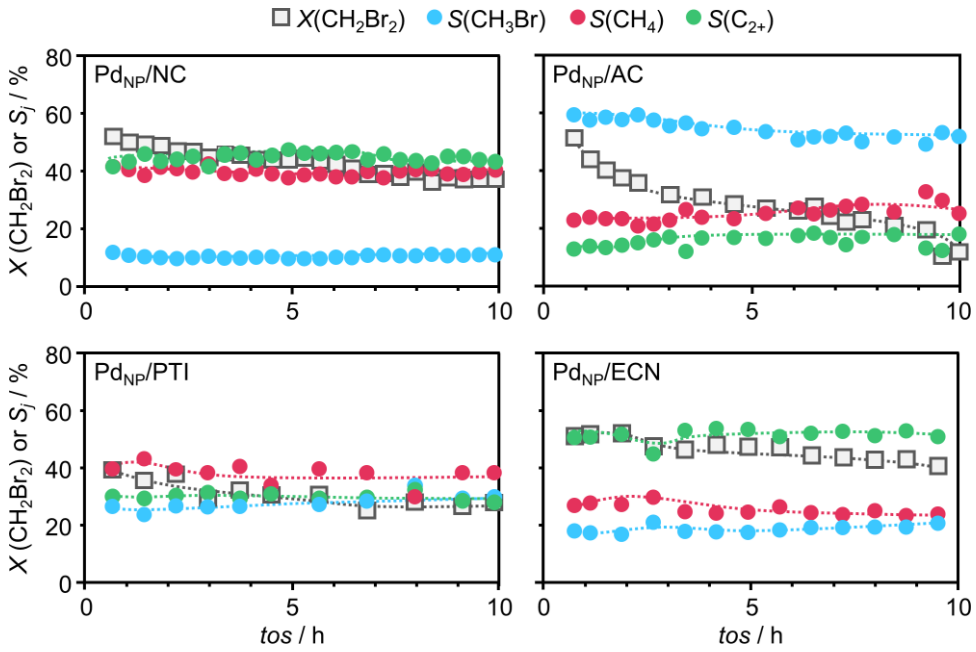

Figure S16. Conversion and product selectivity profiles over Pd NP supported on different carbon-based hosts as a function of time on stream, *tos*. Reaction conditions: CH_2Br_2:H_2:He:Ar = 6:6:83:5, T = 573 K, P = 1 bar, $GHSV$ = 10'800 $cm^3\ h^{-1}\ g_{cat}^{-1}$.

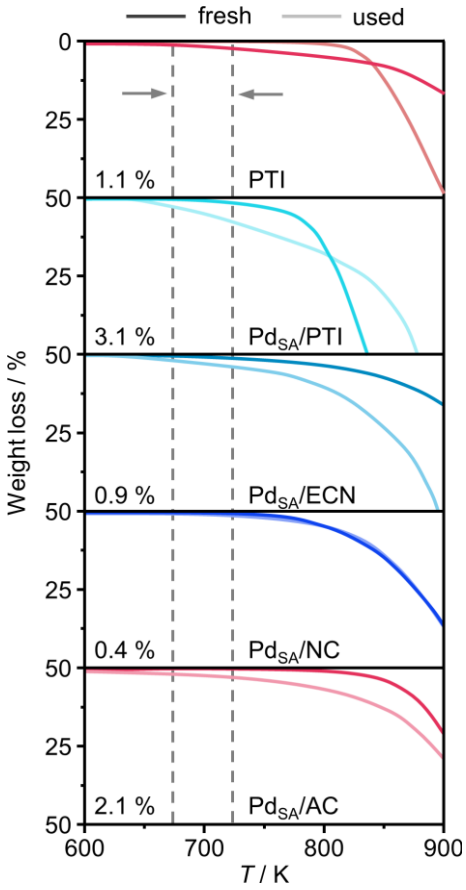

Figure S17. TGA analysis in 20 vol.% O_2/Ar of the Pd SA catalysts, together with the bare PTI support, after 10 h on stream. The amount of coke, reported in the bottom left of each panel, is determined by the difference in the mass loss between the fresh and used catalyst within the temperature range T = 573-723 K, as indicated by the dashed lines.

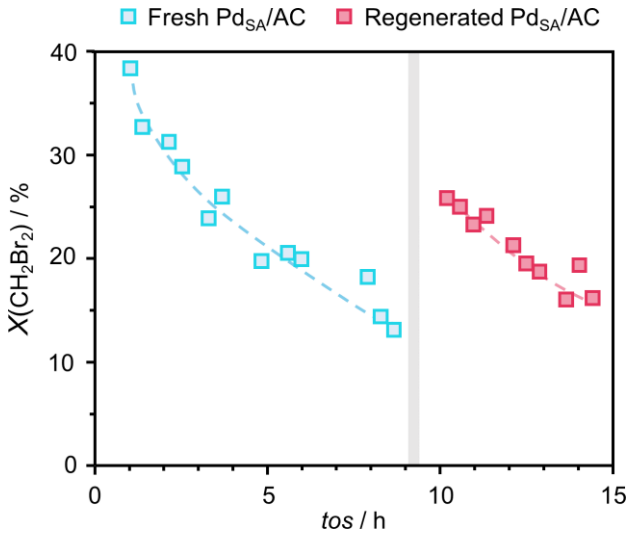

Figure S18. CH_2Br_2 HDB over fresh and regenerated Pd_{SA}/AC. The gray bar corresponds to the regeneration of the catalyst in 20 vol.% O_2/He at 573 K. Hydrodebromination conditions: CH_2Br_2:H_2:He:Ar = 6:6:83:5, T = 573 K, P = 1 bar, $GHSV$ = 10'800 $cm^3\ h^{-1}\ g_{cat}^{-1}$.

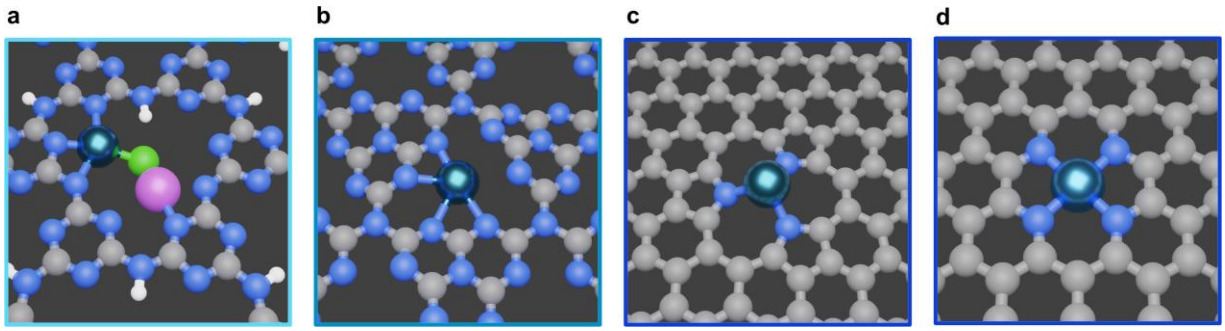

Figure S19. Optimized structures of the Pd active sites for (**a**) Pd_{SA}/PTI, (**b**) Pd_{SA}/ECN, (**c**) Pd_{SA}/NC (3×N5 site), and (**d**) Pd_{SA}/NC (4×N6 site). Structures a-c were used to derive the reaction profiles shown in **Figure 8**. Color code: Pd, metallic blue; C, gray; H, white; N, blue; Li, purple; Cl, green.

References

[1] Faust Akl, D.; Poier, D.; D'Angelo, S. C.; Araújo, T. P.; Tulus, V.; Safonova, O. V.; Mitchell, S.; Marti, R.; Guillén-Gosálbez, G.; Pérez-Ramírez, J., Assessing the Environmental Benefit of Palladium-Based Single-Atom Heterogeneous Catalysts for Sonogashira Coupling. *Green Chem.* **2022,** *24* (18), 6879

[2] Chen, Z.; Mitchell, S.; Vorobyeva, E.; Leary, R. K.; Hauert, R.; Furnival, T.; Ramasse, Q. M.; Thomas, J. M.; Midgley, P. A.; Dontsova, D.; Antonietti, M.; Pogodin, S.; López, N.; Pérez-Ramírez, J., Stabilization of Single Metal Atoms on Graphitic Carbon Nitride. *Adv. Funct. Mater.* **2017,** *27* (8), 1605785

[3] Ding, K.; Derk, A. R.; Zhang, A.; Hu, Z.; Stoimenov, P.; Stucky, G. D.; Metiu, H.; McFarland, E. W., Hydrodebromination and Oligomerization of Dibromomethane. *ACS Catal.* **2012,** *2* (4), 479.